



Prompt fission neutron uranium logging (II): dead-time effect of the neutron time spectrum

Yan Zhang^{1,2} · Chi Liu¹ · Shi-Liang Liu¹ · Hao-Ran Zhang¹ · Hai-Tao Wang¹ · Jin-Hui Qu¹ · Wen-Xing Hu¹ · Ren-Bo Wang¹ · Bin Tang¹

Received: 29 February 2024 / Revised: 24 June 2024 / Accepted: 27 July 2024 / Published online: 9 January 2025

© The Author(s), under exclusive licence to China Science Publishing & Media Ltd. (Science Press), Shanghai Institute of Applied Physics, the Chinese Academy of Sciences, Chinese Nuclear Society 2025

Abstract

The acquisition of neutron time spectrum data plays a pivotal role in the precise quantification of uranium via prompt fission neutron uranium logging (PFNUL). However, the impact of the detector dead-time effect remains paramount in the accurate acquisition of the neutron time spectrum. Therefore, it is imperative for neutron logging instruments to establish a dead-time correction method that is not only uncomplicated but also practical and caters to various logging sites. This study has formulated an innovative equation for determining dead time and introduced a dead-time correction method for the neutron time spectrum, called the “dual flux method.” Using this approach, a logging instrument captures two neutron time spectra under disparate neutron fluxes. By carefully selecting specific “windows” on the neutron time spectrum, the dead time can be accurately ascertained. To substantiate its efficacy and discern the influencing factors, experiments were conducted utilizing a deuterium–tritium (D–T) neutron source, a Helium-3 (³He) detector, and polyethylene shielding to collate and analyze the neutron time spectrum under varying neutron fluxes (at high voltages). The findings underscore that the “height” and “spacing” of the two windows are the most pivotal influencing factors. Notably, the “height” (f_d) should surpass 2, and the “spacing” t_{wd} should exceed 200 μ s. The dead time of the ³He detector determined in the experiment was 7.35 μ s. After the dead-time correction, the deviation of the decay coefficients from the theoretical values for the neutron time spectrum under varying neutron fluxes decreased from 12.4% to within 5%. Similarly, for the PFNUL instrument, the deviation in the decay coefficients decreased from 22.94 to 0.49% after correcting for the dead-time effect. These results demonstrate the exceptional efficacy of the proposed method in ensuring precise uranium quantification. The dual flux method was experimentally validated as a universal approach applicable to pulsed neutron logging instruments and holds immense significance for uranium exploration.

Keywords PFNUL · Neutron time spectrum · Dead time · Pulsed source · Correction method

1 Introduction

Uranium is a critical strategic resource in China, and it is significant demand for applications such as nuclear power generation. Therefore, uranium exploration is crucial to

ensuring a stable supply of uranium resources in China. Nuclear well logging is an efficient exploration method in the fields of energy and mineral exploration, including uranium and petroleum, and it occupies a paramount position in the well logging industry [1, 2]. Nuclear well logging primarily comprises gamma-ray, neutron, and nuclear magnetic resonance logging [3–6]. In the exploration of uranium, China has traditionally employed natural gamma-ray logging (either total count or spectrum) for uranium quantification [7, 8]. However, this approach suffers from drawbacks, such as low drilling efficiency, high exploration costs, and long uranium quantification cycles [9]. Prompt fission neutron uranium logging (PFNUL) technology can effectively utilize the fission reaction of uranium to survey underground

This work was supported by the National Natural Science Foundation of China (No. 42374226), Jiangxi Provincial Natural Science Foundation (Nos. 20232BAB201043 and 20232BCJ23006), Nuclear Energy Development Project (20201192-01), National Key Laboratory of Uranium Resource Exploration-Mining and Nuclear Remote Sensing (ECUT) (2024QZ-TD-09), and Fundamental Science on Radioactive Geology and Exploration Technology Laboratory (2022RGET20).

Extended author information available on the last page of the article

uranium elements and thereby offer the advantages of direct measurements and accurate resolution [10]. PFNUL utilizes a pulsed neutron source, such as a D–T neutron source, to emit pulsed neutrons and bombard the formation. If the formation contains uranium elements, then the neutrons react with the uranium elements to produce fission neutrons that impact the neutron time spectrum results [11]. By collecting the pulse neutron time spectrum information, relevant information can be extracted to quantitatively analyze the uranium elements in the formation [12–14]. However, a pulsed neutron source can emit a high yield of neutrons in microseconds or tens of microseconds, which could briefly saturate the neutron detector and lead to a significant dead-time effect that could severely impact the accuracy of a quantitative analysis [15–18]. Therefore, under high neutron yield conditions, the collection of the pulse neutron time spectrum and dead-time correction are urgent challenges that need to be addressed in neutron uranium well logging.

In PFNUL, ^3He gas detectors are preferred for neutron time spectrum acquisition because of their high detection efficiency and compact size. However, similar to GM tubes, they face challenges related to their gas response speed, particularly at elevated neutron fluxes, where they are unable to differentiate between two or more neutron events occurring in short time intervals [19, 20]. This phenomenon, known as the dead-time effect [21–23], generates an abundance of dead time and consequently impacts the accurate detection of the neutron time spectrum. The primary sources of the dead-time effect include the intrinsic characteristics of the detector and pulse analysis circuit characteristics. These factors may introduce systematic biases into the experimental results, particularly in situations involving short pulses and high neutron fluxes, where dead time can distort the neutron time spectrum and affect the accuracy of the experimental results. Therefore, it is crucial to conduct a thorough study of the dead-time effect on ^3He detector systems in neutron uranium well logging [24].

In the 1970s, scholars devoted considerable research efforts to the dead-time problem by introducing two widely employed dead-time models: extended and non-extended [25, 26]. Simone et al. applied a two-source method in conjunction with the principle of conformal measurements to compute the systematic dead time of a ^3He detector [27]. Furthermore, David et al. harnessed the versatility of the pulse arrival time recording module (PATRM) to observe the dead time of a ^3He detector while recording slow fission neutrons emitted from small, fissionable materials irradiated by an intense neutron source [28]. Akyurek generated a neutron beam using the Missouri University of Science and Technology research reactor and measured the count rate under various conditions by introducing different shielding thicknesses to the ^3He detector. The count rates under different scenarios were measured with varying shielding

thicknesses, and the dead times for both ^3He extended and non-extended models were calculated. These results were achieved by combining Monte Carlo N-particle (MCNP) simulations with the decay law [29]. The dead time of the NaI detector was determined using the decay law [30–32]. Hashimoto employed the variance-to-mean method to calculate the dead times of neutron detectors, including ^3He and BF₃. The calculated dead times for the two neutron detectors LND-251 and LND-2524 were determined to be $7.5 \pm 0.54 \mu\text{s}$ and $8.31 \pm 0.5 \mu\text{s}$, respectively [33, 34].

In conclusion, the principal approaches to studying dead-time effects in neutron detectors can be summarized into two sources: the decay source, reactor power, and variance-mean methods. These methods effectively corrected and validated the dead time generated by the ^3He detector in various scenarios. Among them, the two-source method is straightforward to implement and suitable for basic dead-time measurements that can be completed in a relatively short period using two sources of known activity. However, the two-source method relies on the difference in source activity and may be more accurate for substantial differences in activity but less accurate for similar activities. Hence, this method is not suitable for intricate systems, and, for more precise measurements, the source placement and experimental conditions may require adjustments that increase the experimental complexity. The decaying radioactive source method applies to systems involving radioactive decay and not to systems without decay, and it may be susceptible to statistical errors over short measurement times [35]. The reactor power method is applicable to scenarios with high-intensity radiation, such as nuclear reactors, and it requires measurements in a radioactive environment, which presents heightened safety and technical challenges [36], as few laboratories have timely access to neutron irradiation facilities. The variance-mean method applies to all types of systems, including scenarios involving statistical measurements; however, it requires more sophisticated data processing and may require longer data acquisition times to attain accurate results.

However, these studies could not effectively measure and correct the dead-time characteristics of PFNUL instruments. Therefore, the development of a new method for calculating and correcting dead time specifically tailored to pulsed neutron uranium well logging instruments is urgently required. PFNUL instruments commonly utilize D–T pulsed neutron generators in which the neutron yield can be controlled by high pressure to adapt to different detectors and experimental requirements [37]. By exploiting the adjustable neutron flux capabilities of the PFNUL instruments, this study, based on the theory of dead-time effects, derives a dead-time extraction method using the dual flux method (DFM) for the pulsed neutron time spectrum [38]. The effectiveness and accuracy of this method were validated through

a series of experiments. Additionally, a correction formula for the dead-time effects was derived, based on the neutron decay law. Finally, the acquired neutron time spectrum was corrected for dead-time effects. A comparison of the decay coefficients before and after correction reveals a significant reduction in deviation, compared with the MCNP simulation decay coefficients [39, 40]. This reduction more accurately reflects the true information of the neutron time spectrum and lays the foundation for precise uranium quantification in PFNUL. Thus, the proposed method is of paramount significance in this context.

2 Dual flux method and theory

2.1 Dead-time calculation formula derivation

The principal contributor to the dead time of the ³He neutron detector is the detector itself. In the process of detecting neutrons, because neutrons are not charged and cannot directly cause the “ionization” or “excitation” of the material, the neutron signal pulse is a neutron reaction with ³He to generate protons, emit tritium nuclei in the opposite direction, and cause the ³He gas to ionize to form a large number of ion pairs (electrons and positive ions). A ³He tube with a high voltage of the anode filament and ³He tube shell form an electric field. Under the action of the electric field, the electrons and positive ions drift to the anode filament, to the wall of the cathode tube, and, ultimately, through a series of anode filament reactions to produce an effective neutron signal. Therefore, the pulsed signal from a neutron must undergo a series of processes before it can be recorded. Figure 1 illustrates the reason for dead-time generation: If the ³He detector system comes with another neutron pulse signal during signal processing, it will produce pulse superposition. Therefore, the pulse signal cannot be processed in time and misses counting, which is the main reason for non-expanded dead-time generation. Scholars have proven that most of the contribution of the dead time of the ³He detector comes from non-expanded dead time. Related scholars have proven that most of the dead time of the ³He detector comes from the non-expanded dead time. Therefore, the model used in

this experiment refers to the non-expanded dead time. The ³He detector can be synchronized with the pulse signal of the pulsed neutron generator through the digital multi-channel collector and record the time distribution curve of the number of neutrons after the neutron pulse is discharged, which ultimately forms the required neutron time spectrum. The counts at each moment, corresponding to time t_0 , are converted to count rates before processing the neutron time spectrum. The conversion equation is represented by Eq. (1).

$$n_i = \frac{N_i}{t \times f \times t_0} \quad i = 1, 2, 3 \dots \tag{1}$$

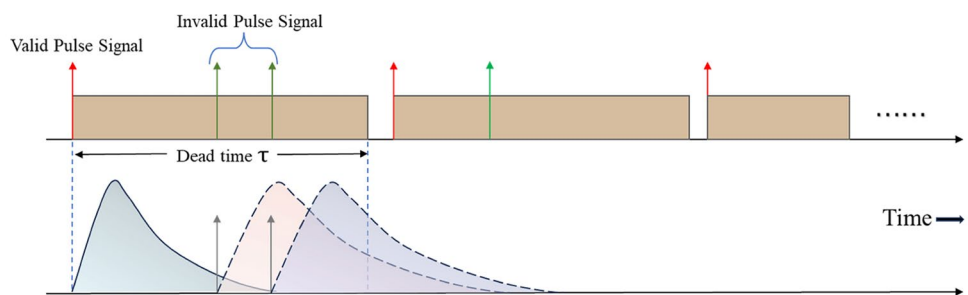
where n_i is the count rate normalized to the i channel, N_i is the count corresponding to the i channel in the neutron time spectrum, t is the acquisition time of the detector, f is the frequency of the pulsed neutron source, and t_0 is the time corresponding to the i channel. After processing Eq. (1), we obtain a revised neutron time spectrum.

In the neutron field of a pulsed source, the average number of true neutrons incident on the ³He detector per unit time is m , the number of neutrons recorded per unit time is n , and the dead time of the detector is τ . The dead time of the ³He detector is denoted by $n\tau$, and the total number of counts lost owing to dead time is $mn\tau$, which is the number of counts lost. Subsequently, τ can be obtained from Eq. (2) and is written as follows:

$$\tau = \frac{m - n}{mn} \tag{2}$$

As shown in Fig. 2, two neutron time spectra detected by the ³He ratio counting tube were selected, and two windows of the same size were set up with window widths defined as t_{ww} , which can be set to 2 μ s, 8 μ s, 16 μ s, 24 μ s, or 32 μ s. The initial time of window 1 (W1) should start when the count rate is high and unrelated to the source neutrons. The time W1 from the peak of the neutron time spectrum is the delay time T_0 . The initial time of window 2 (W2) should be far away from W1, and the interval between the two time windows is denoted by t_{wd} . The ratio of the count rates of the two time spectra within the window is denoted by f_d , used to measure the height of the time window, and subsequently

Fig. 1 Dead-time generation process



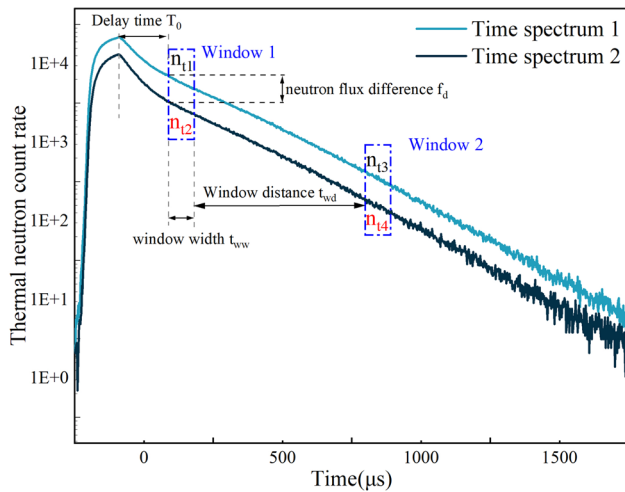


Fig. 2 (Color online) Parameters related to setting the time window on the neutron time spectrum

discussed in detail. The position of W1 is at moment $t1$ of the neutron time spectrum. Then, $t1$ is equal to $t2$, and the corresponding neutron count rates of the high- and low-flux neutron time spectra are n_{t1} and n_{t2} , respectively. Moreover, $f_{d1} = n_{t1}/n_{t2}$, and the corresponding real count rates are m_{t1} and m_{t2} . The position of W2 is at the $t3$ moment of the neutron time spectrum. Then, $t3$ is equal to $t4$, corresponding to the high- and low-flux neutron time spectra of the neutron count rates of n_{t3} and n_{t4} , respectively. Then, $f_{d2} = n_{t3}/n_{t4}$, and the corresponding true count rate is m_{t3} , m_{t4} .

Evidently, in a neutron time spectrum devoid of dead-time effects, the ratio of the neutron count rates for any two captured windows should be equal. The ratio of the true count rate can be expressed as follows:

$$\frac{m_{t1}}{m_{t2}} = \frac{m_{t3}}{m_{t4}} \tag{3}$$

Combining Eqs. (3) and (2), the τ term can be written as follows:

$$\tau = \frac{n_{t1}n_{t2} - n_{t3}n_{t4}}{n_{t1}n_{t4}(n_{t2} + n_{t3}) - n_{t3}n_{t2}(n_{t1} + n_{t4})} \tag{4}$$

The only unknown parameter is the true count rate m . The detector dead time can be determined by equating the two sets of count rates from the experimental tests in Eq. (4).

2.2 Dead-time correction

Finally, the formula for the dead time τ is introduced into the equation for the relationship between the true count n and count m detected by the ^3He detector as well as the dead time τ described in Eq. (2) and combined with Eq. (1). The

correction formula for the true count m_i can be obtained as follows:

$$m_i = \frac{n_i}{1 - n_i\tau} = \frac{n_i}{1 - n_i \frac{n_{t1}n_{t2} - n_{t3}n_{t4}}{n_{t1}n_{t4}(n_{t2} + n_{t3}) - n_{t3}n_{t2}(n_{t1} + n_{t4})}}, \quad i = 1, 2, 3 \dots \tag{5}$$

where n_i corresponds to the count corresponding to each tract site in the neutron time spectrum, and m_i is the corrected true count for that tract site.

3 Experiment

3.1 Experimental parameters

The experiment uses a variety of specifications of small, sealed neutron tubes that were independently developed and produced. Moreover, this experiment adopts the Penning Ion Source Technology, which vacuum packages the ion source, acceleration system, target, etc., and accelerates the target after the ionization of deuterium and tritium mixed gases. The deuterium and tritium nuclear reaction occurs on the target membrane to generate neutrons. Hence, the neutron flux generated can be controlled by controlling the size of the target's high voltage. The neutron yield of the D-T neutron tube is up to 1×10^9 n/s, which meets the requirements of this experiment. Moreover, the working life under the maximum yield is ≥ 300 h, which can withstand a 175°C high-temperature environment. The neutron generator has two modes of operation: pulse and direct current (DC). This experiment used a pulse mode with a pulse period of $2000 \mu\text{s}$ and pulse width of $200 \mu\text{s}$ that can stably emit 14.1 MeV fast neutrons in the 4π direction. The neutron detector used in this experiment was a Global Nucleonics 15He3-304-38FS-type ^3He positive ratio counting tube. The ^3He tube and neutron generator, together with the polyethylene barrel, were set into a $163 \text{ cm} \times 203 \text{ cm} \times 166 \text{ cm}$ polyethylene shielding body at the center of the hole with a depth of 120 cm and radius of 6 cm . The shield can quickly slow the emitted fast neutrons. Its geometric position is shown in Fig. 3a. This experiment uses a digital multi-channel acquisition board (DCMA) for the acquisition of the neutron time spectrum [41, 42]. The neutron generator pulse synchronization signal is connected to the multi-channel board synchronization signal, and the detection time is synchronized with the pulse neutron emission time of the neutron generator so that it can collect neutrons emitted within $200 \mu\text{s}$ within $2000 \mu\text{s}$ of the neutron attenuation. The multi-channel acquisition board sends the data to the upper computer software via RS485, the upper computer software completes the acquisition and preservation of the neutron time spectrum, and Fig. 3b [43]

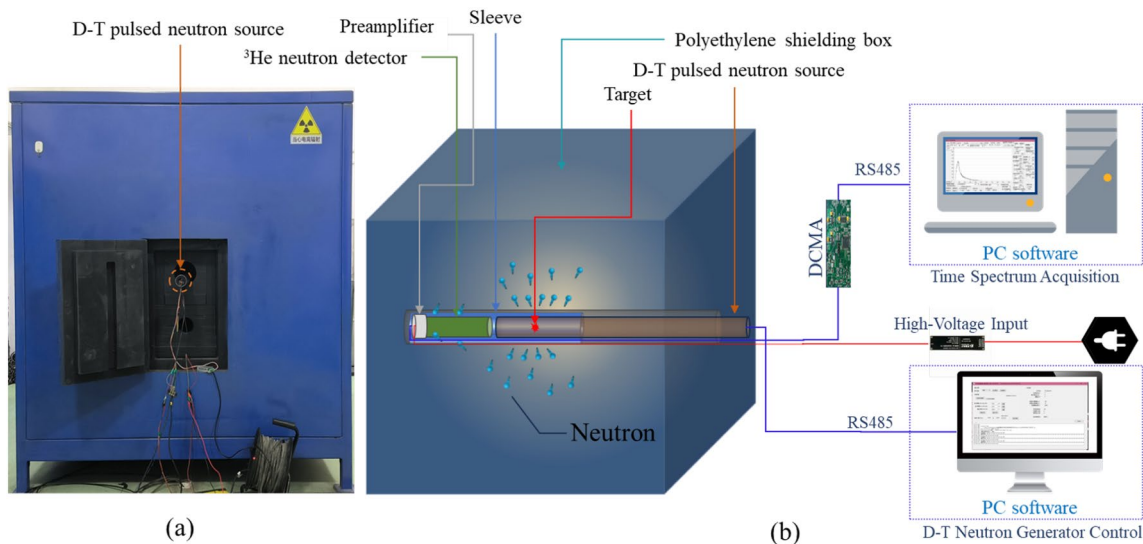


Fig. 3 (Color online) **a** Physical diagram of the experimental apparatus. **b** Schematic of the experimental setup

shows the neutron time spectrum acquisition process. In this study, Monte Carlo N-Particle (MCNP) software was used to simulate the neutron transport and interaction process inside a polyethylene shield, which is a powerful Monte Carlo simulation tool that is widely used in the fields of nuclear physics, medical radiation therapy, and radiation protection. This method is used to simulate the neutron time spectrum of the experimental environment in an ideal situation for comparison with experimental and corrected results [44]. Thus, the neutron time spectrum was used to compare and verify the experimental and corrected results. Finally, a neutron time spectrum correction experiment of the PFNUL instruments was conducted in a standard model well in a uranium mine.

3.2 Experiment procedure

The experimental measurements involved neutron time spectrum measurements under five different neutron fluxes by controlling a D–T neutron generator. The parameters for each experimental group were as follows. After setting the target high pressure for the first experimental group, neutron

time spectrum data collection was initiated when the neutron generator’s target high pressure was stabilized. A data collection duration of 300 s was employed, and three sets of neutron time spectrum data were collected at the same target high pressure. The average of the three sets was used as the effective test result for that particular group. Following the completion of each experiment, the target high pressure was adjusted for the next experimental group, and the process was repeated accordingly. Table 1 lists the parameter configurations of each experimental group.

Figure 3a shows the experimental setup. The MCNP method was used to establish the Monte Carlo model. The model illustrated in Fig. 3b consists mainly of a D–T neutron source, polyethylene shielding box, sleeve, and ³He detector. The D–T neutron source was approximated as a point source emitting 14.1 MeV fast neutrons in the 4π direction with a pulse period of 2000 μs and a pulse width of 200 μs, aligned with the parameters of the actual experimental setup. The simulation utilized element cross-section data from the NDF/B-VIII.0 database, and ultimately, theoretically

Table 1 Detailed parameterization of the experiment

Experiment no.	Target high voltage (kV)	Pulse period (μs)	Pulse width (μs)	Wide time spectrum channel (μs)	Number of measurement	Single measurements time (s)
#1	40	2000	200	2	3	300
#2	50					
#3	60					
#4	70					
#5	80					

simulated data for the experimental thermal neutron time spectrum were obtained.

By employing a ^3He detector, neutron counts were recorded at varying target voltages. The discrepancies in the neutron decay coefficients within the neutron time spectrum under different target voltages were ascribed to count losses stemming from the dead time. The detector dead time was estimated using Eq. (4).

4 Results and discussion

Figure 4 shows the neutron time spectrum obtained by the neutron generator at distinct high target voltages. According to the neutron diffusion theory, the decay contribution of the neutron time spectrum measured in the borehole consists of two parts: the borehole and the stratum. At the beginning of the borehole, the rapid diffusion of the neutrons in the borehole decays, leading to a fast decay of the neutron time spectrum for some time immediately after the end of the neutron pulse. Then, the decay rate becomes stable, and the decay contribution of the neutron time spectrum at this time mainly comes from the stratum, whereas the decay contribution mainly comes from the formation. At the target high voltage of 80 kV, the neutron time spectrum is partially deformed, owing to the loss of the neutron count rate in the high count rate period after the end of the neutron pulse, owing to the effect of dead time. According to the dead-time calculation method deduced above, considering that the relevant parameters of the time window may have a large impact on the dead time, the following analysis of the impact of different window parameter sets on the dead time

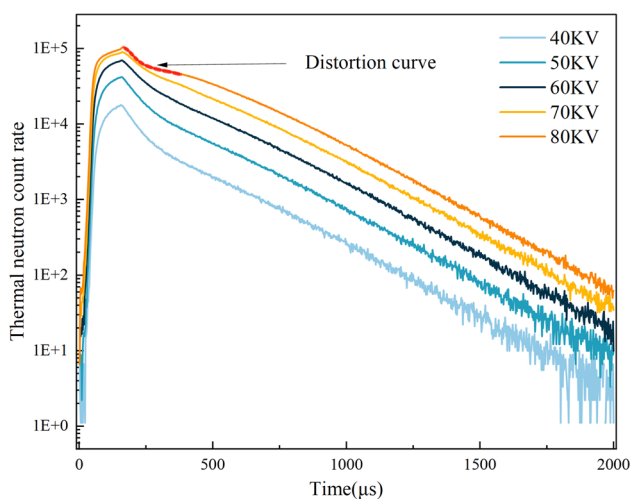


Fig. 4 (Color online) Neutron time spectrum measured at different target high voltages

was conducted to determine the window parameters suitable for the dead-time calculation method.

4.1 Effect of window settings on dead time

4.1.1 Window height

The window height f_d , delineated as the disparity between the two neutron time spectrum curves at identical positions, must adhere to the theory, ensuring a substantial difference. Evaluating the neutron time spectrum curves corresponding to different target high pressures, four distinct window heights were chosen, and their combinations are enumerated in Table 2. Notably, the amalgamated height f_d exhibited a decreasing trend.

4.1.2 W1 initiation time

Considering that the pulse width of the neutron emitter is 200 μs , the simulation results demonstrated that it takes approximately 150 μs for all the source neutrons to be converted into thermal neutrons. Therefore, the initiation time of W1 is set to approximately 400 μs to avoid the influence of the source neutrons. The initiation time of W1 is shown in Fig. 5, which shows that after 400 μs , the dead-time calculation results of the combinations tend to stabilize. Hence, it is recommended to set the initiation time of W1 to 400 μs .

4.1.3 Window width

The window width, t_{ww} , denotes the temporal span between the commencement and cessation instants of the time window. The pulse width of the neutron generator was set to 200 μs to obviate the influence of the source neutrons and aperture effect. Based on the calculation principle, the initiation time of W1 was designated as 400 μs . Then, W2 commenced at 800 μs , maintaining a separation of 400 μs between the two windows (t_{wd}). Defining four distinct t_{ww} values requires

Table 2 Selection of four combinations of different neutron flux differences in the neutron time spectrum. Here f_{d1} and f_{d2} are the ratios of the neutron fluxes of the two neutron time spectra within W1 and W2

	Time spectrum combination	f_{d1}	f_{d2}
Height I	#1 + #5	14.83	19.42
Height II	#2 + #5	5.37	6.63
Height III	#3 + #5	2.56	3.13
Height IV	#4 + #5	1.43	1.67

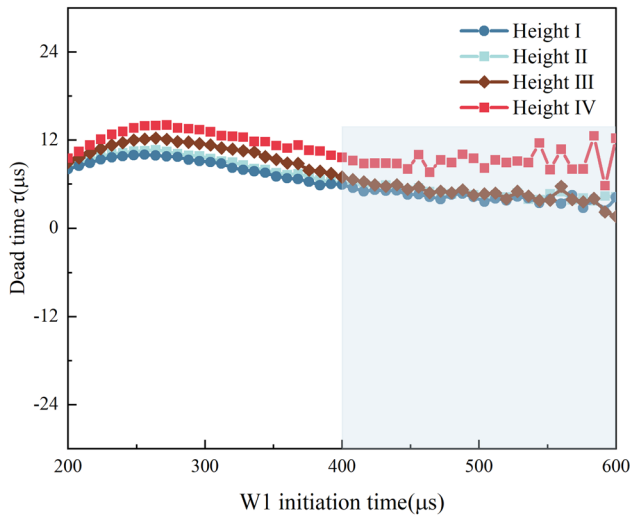


Fig. 5 Changes in dead time with an initial time shift of W1

adopting a neutron time spectrum channel width of 8 μs. Table 3 lists the commencement times and widths of each window.

Table 4 presents the count rates of the neutrons under various high target voltages corresponding to the four t_{ww} values of the two windows.

4.1.4 Dead-time calculations

Based on Eq. (4), the dead time was calculated for different t_{ww} by varying f_d as mentioned above. Figure 6a presents the results. Different t_{ww} values have little effect on the dead time at the same height. Moreover, #4 + #5 and other groups of calculation results differ because the two high voltages

are too close, and the dead-time calculation method utilizes the difference between the effect of the dead time on the time spectrum and the time spectrum without the effect of dead time. The time spectrum at a high voltage of 70 kV is relatively more affected by dead time, which causes minimal differences in the two neutron time spectra, ultimately resulting in inaccurate findings. Therefore, according to the size of the f_d parameter of each group, the selection of the height must be constrained. That is, the f_d should be greater than 2 as far as possible.

4.2 The effect of two-window spacing t_{wd} on dead-time calculations

Here t_{wd} denotes the time interval between W1 and W2. The initiation channel of W1 was set to 400 μs to mitigate the effect of statistical fluctuations in the data when the count rate was extremely low. The channel of W2 was incremented from 400 μs to 1000 μs in steps of 10 μs, with the t_{ww} fixed at 8 μs. Figure 6b elucidates the corresponding variation in dead time for two window intervals ranging from 0 μs to 600 μs. These results are consistent with those previously mentioned. Moreover, the distance between two windows should not be extremely small. Notably, the dead time tended to stabilize when the interval between the two windows exceeded 200 μs. Table 5 lists the average values of the dead time in the stable interval. The determined dead time of the ³He detector system aligns closely with the ³He tube dead time calculated by Hashimoto using the variance-mean method (Feynman- α).

Table 3 Time window width settings

No.	W1			W2		
	Threshold	Terminal	t_{ww} (μs)	Threshold	Terminal	t_{ww} (μs)
1	400	408	8	800	808	8
2	400	416	16	800	816	16
3	400	424	24	800	824	24
4	400	432	32	800	832	32

Table 4 Neutron count rates for two windows with different window widths at different target pressures, where window 1 is expressed as W1 and window 2 is expressed as W2

t_{ww} (μs)	#1		#2		#3		#4		#5	
	W1	W2								
	$\times 10^3$	$\times 10^2$	$\times 10^3$	$\times 10^3$	$\times 10^4$	$\times 10^3$	$\times 10^4$	$\times 10^3$	$\times 10^4$	$\times 10^4$
8	3.00	6.18	8.28	1.78	1.74	3.84	3.12	7.19	4.45	1.20
16	2.95	5.99	8.11	1.72	1.71	3.79	3.08	7.07	4.41	1.18
24	2.89	5.95	7.99	1.69	1.69	3.72	3.03	6.98	4.38	1.16
32	2.84	5.91	7.87	1.66	1.66	3.66	2.99	6.89	4.33	1.15

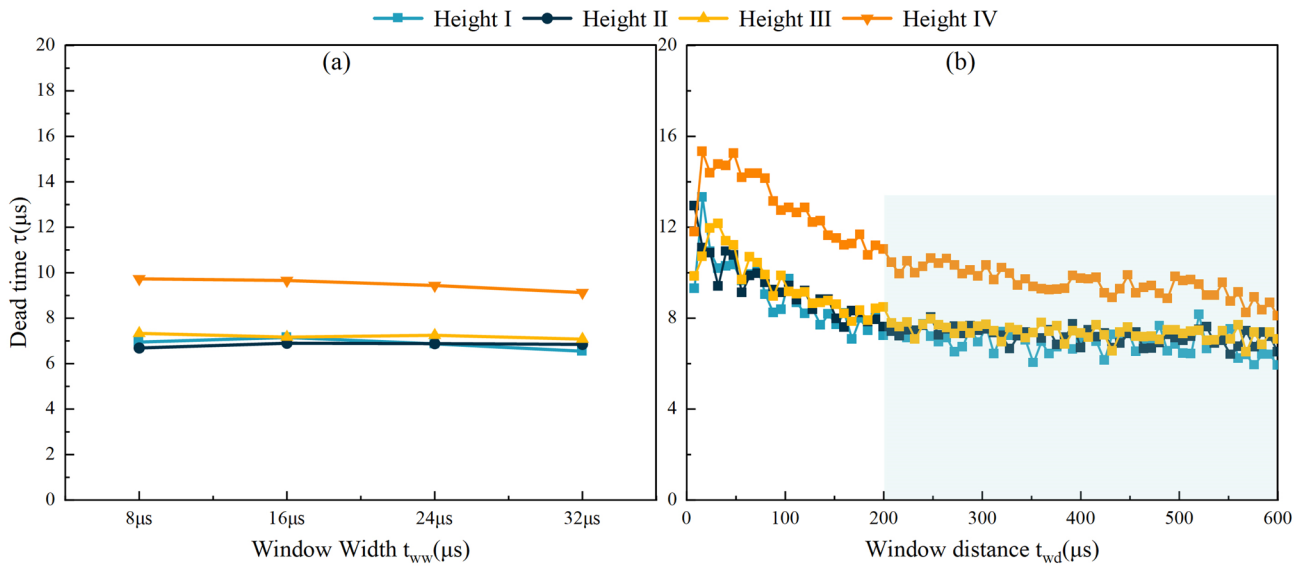


Fig. 6 (Color online) **a** Dead-time comparison for different window widths at four window heights. **b** Changes in dead time with gradually increasing spacing between two time windows for different values of f_d

4.3 Correction of neutron time spectrum and MCNP validation

Under identical experimental conditions, the neutron decay process is expressed as follows:

$$N = N_0 e^{-\frac{t}{\mu}}, \tag{6}$$

where N_0 is the neutron density after a delay time of T_0 after a single neutron emission, and the delay time of T_0 eliminates the influence of the aperture effect such that the decay of neutrons is only affected by a single stratum. Additionally, t is the beginning time of the T_0 moment, and μ is the neutron decay constant in microseconds.

Then, m can be written as follows:

$$\begin{cases} m_{t1} = N_1 e^{-\frac{t1}{\mu1}} \\ m_{t2} = N_2 e^{-\frac{t2}{\mu2}} \\ m_{t3} = N_1 e^{-\frac{t3}{\mu1}} \\ m_{t4} = N_2 e^{-\frac{t4}{\mu2}} \end{cases} \tag{7}$$

It follows from Eq. (3) that

$$\frac{m_{t1}}{m_{t2}} = \frac{m_{t3}}{m_{t4}} \stackrel{\text{equivalence}}{\implies} \frac{m_{t1}}{m_{t3}} = \frac{m_{t2}}{m_{t4}}. \tag{8}$$

Combining Eqs. (7) and (8), the equation can be written as follows:

$$e^{-\frac{t1-t3}{\mu1}} = e^{-\frac{t2-t4}{\mu2}}. \tag{9}$$

Here, $t1 - t3 = t2 - t4$. Thus, $\mu1 = \mu2$, and the attenuation coefficients of our two measurements for different numbers of neutrons should be equal.

Based on the relationships expressed in Eq. (5) between the actual counts, observed counts, and dead time, a detailed correction of the observed counts was performed using the previously calculated dead-time values. Figure 7a–d illustrates the correction effects. Notably, the dead-time correction result for Height IV exhibits a negative outlier, according to the dead-time formula and related theories. Hence, the dead-time results do not match the theoretical results [45]. This theoretical derivation implies that the neutron attenuation coefficients with varying fluxes should be uniform [46]. Accordingly, a negative exponential fit was employed, and the fitting equations are shown in Eq. (10) on the linear decay curves in linear coordinates. This fit was conducted both before and after dead-time correction, considering different heights. The fitting range was chosen as $400 \mu\text{s} - 2000 \mu\text{s}$ to eliminate the influences of source neutrons [47].

Figure 8a–d presents the fitting results, where Fig. 8a illustrates the results before correction, and Fig. 8b–d illustrates the fitting outcomes after dead-time correction for Heights I–III. Moreover:

$$y = N_0 e^{-\frac{t}{\mu}} + y_0. \tag{10}$$

The addition of y_0 to Eq. (10) represents the background noise.

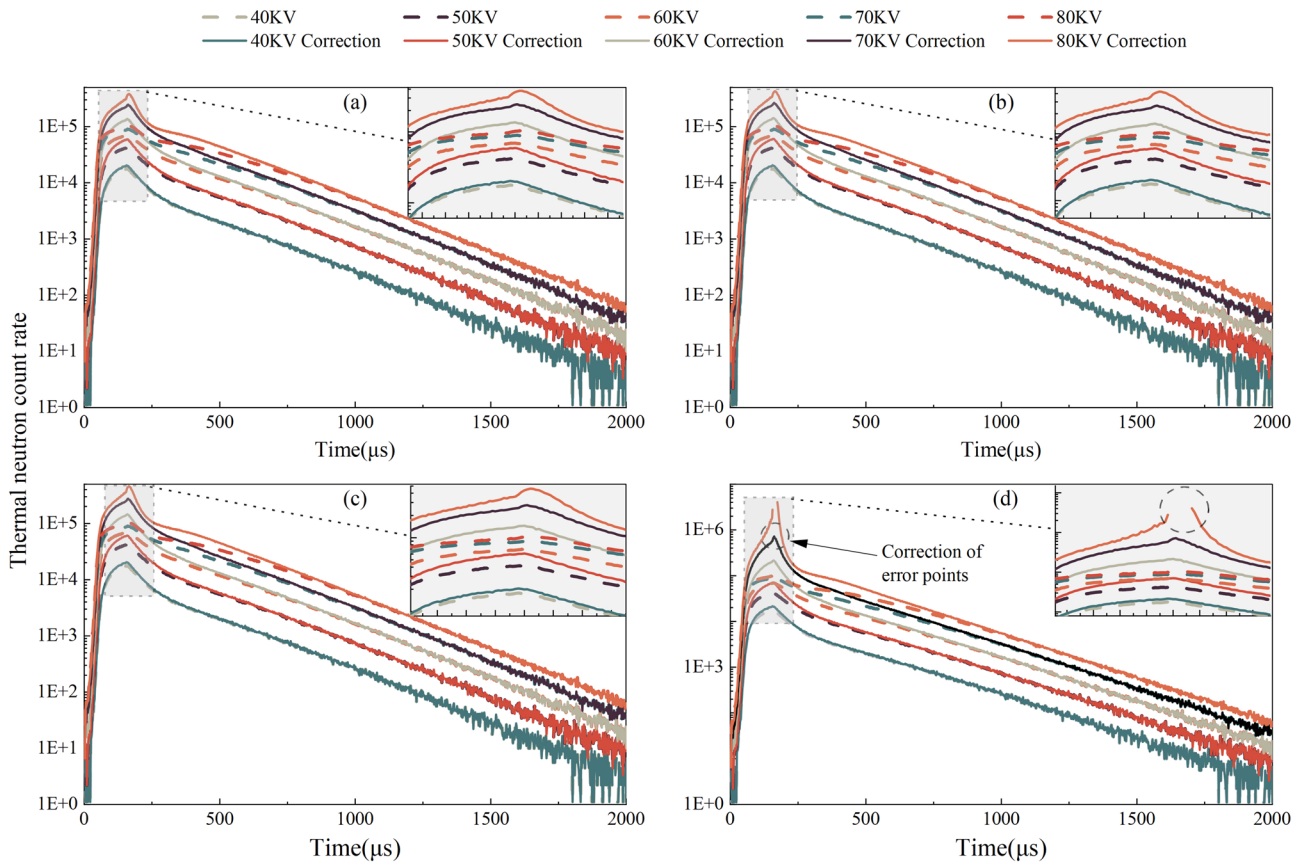


Fig. 7 (Color online) **a** Height I dead-time correction results. **b** Height II dead-time correction results. **c** Height III dead-time correction results. **d** Height IV dead-time correction results

Table 5 Mean values of dead time in stabilization intervals at four altitudes

	τ (t_{wd} 200 μ s–600 μ s average value)
Height I	7.06 μ s
Height II	7.35 μ s
Height III	7.52 μ s
Height IV	9.76 μ s

The attenuation coefficient of the time spectrum fit for the MCNP simulation is 237.5 ± 0.8 , and the precision of the correction effect is quantified by computing the relative deviation (*RD*) of the attenuation coefficients of the neutron time spectrum before and after correction from the MCNP simulation, as indicated in Eq. (11) [48, 49]:

$$RD = \frac{|X_{av} - X_{mc}|}{X_{mc}} \times 100\% \tag{11}$$

where X_{av} is the value of μ before and after dead-time correction, and X_{mc} is the value of μ_{mc} for MCNP simulation.

In the data presented in Table 6, it is evident that the decay coefficients of each curve closely align after correction, aligning with the conclusion that the deduced decay coefficients are consistent. Comparing the pre-correction and post-correction attenuation coefficients with the MCNP simulation results, it is apparent that Height I, Height II, and Height III exhibit favorable correction effects. The *RD* is 12.4% before correction, reduced to approximately 5% after correction.

4.4 Application in PFNUL

PFNUL instrument is used for pulsed neutron uranium quantitative logging, using pulsed neutrons to trigger the fission reaction of uranium (^{235}U) element in the formation [50–52], detecting and extracting the transient neutron time spectrum generated by the fission of uranium, and then realizing the rapid detection of uranium in drilling holes and uranium quantification. Especially for the method technology of uranium fission information based on the ratio of epithermal neutrons to thermal neutrons with a double neutron time spectrum, the accuracy of the detection of thermal

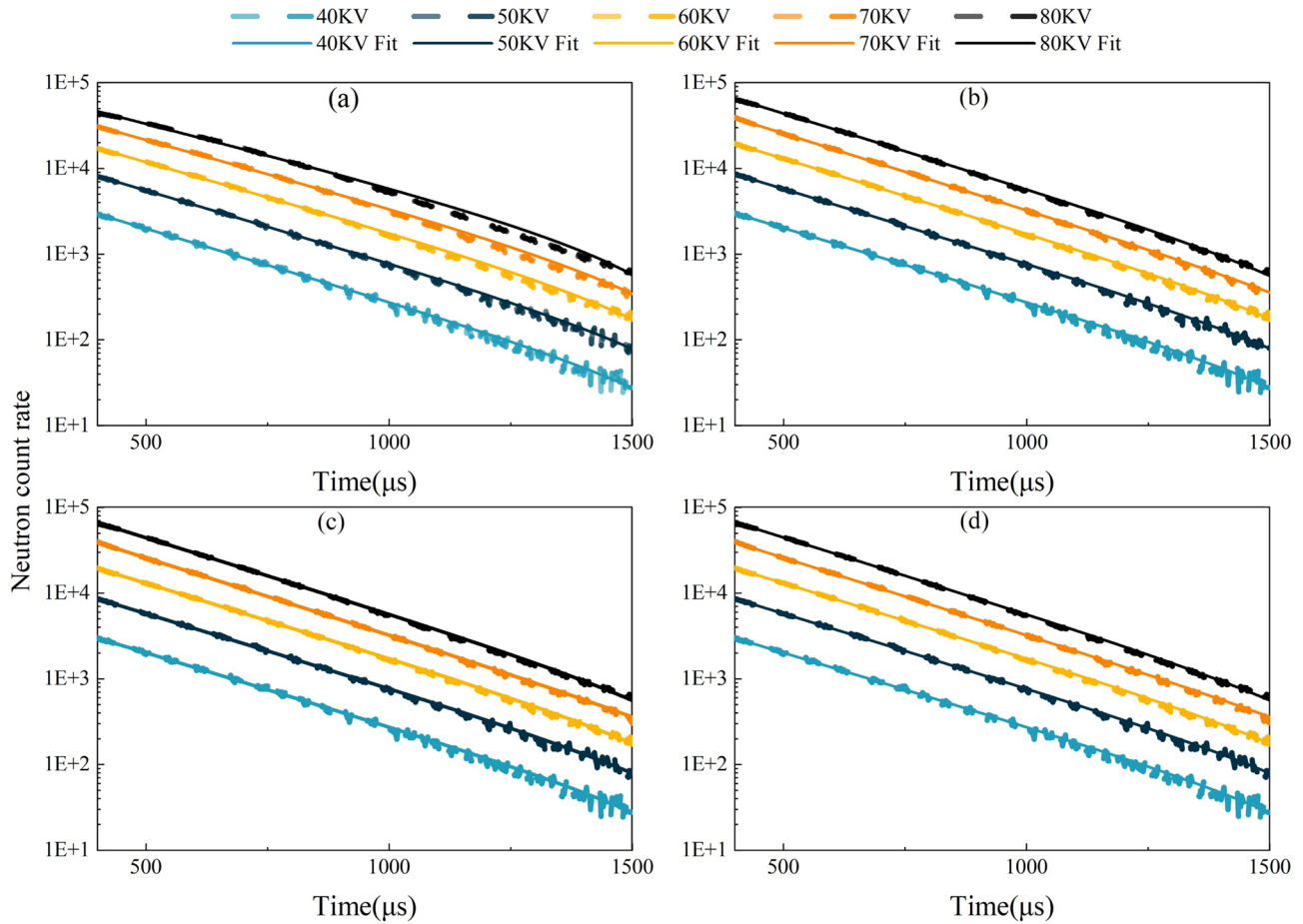


Fig. 8 (Color online) **a** Fitting results before correction. **b** Fitting results after the dead-time correction for Height I. **c** Fitting results after the dead-time correction for Height II. **d** Fitting results after the dead-time correction for Height III

Table 6 Comparison of fitted parameters before and after correction. Correction I-III corresponding to the Heights I-III dead-time correction

High voltage (kV)	Pre-correction		Correction I		Correction II		Correction III	
	μ_{pre}	RD_{pre} (%)	μ_I	RD_I (%)	μ_{II}	RD_{II} (%)	μ_{III}	RD_{III} (%)
40	257.7	8.5	254.9	7.3	254.8	7.3	254.8	7.3
50	259.6	9.3	251.9	6.1	251.6	5.9	251.4	5.9
60	268.3	13.0	251.2	5.8	250.5	5.5	250.1	5.3
70	277.0	16.6	244.2	2.8	242.7	2.2	241.9	1.9
80	301.1	26.8	248.9	4.8	246.5	3.8	245.1	3.2
Average value	272.7	12.4	250.2	5.4	249.2	4.9	248.7	4.7

neutrons will have a direct impact on the accuracy of uranium quantification [53–56]. Finally, the corrected method and the dead-time results were made in the uranium fission transient neutron logging instrument, as shown in Fig. 9, for the collection of two different sources under high target pressure in the same uranium model well with a neutron generator under controlled target pressure. The neutron time spectrum under neutron flux are original spectrum 1 and original spectrum 2, respectively, and it can be seen that the

count rate of the original neutron time spectrum 1 and the original neutron time spectrum 2 before correction is low due to the dead-time problem, for a period of time at the end of the pulse, since the neutron count rate is high at this time, again the effect of dead time is the largest, so a significant correction effect of dead time can be observed for this period of time, and as the neutron count rate decreases, the effect of dead time also decreases, so the correction effect of dead time decreases with the decrease in the neutron count

Table 7 Comparison of attenuation coefficients before and after correction

μ^*	Original	<i>RD</i>	After corrected	<i>RD</i>
spectrum1	215.3±0.9	22.94%	182.9±0.7	0.49%
spectrum2	264.7±1.5		183.8±0.6	

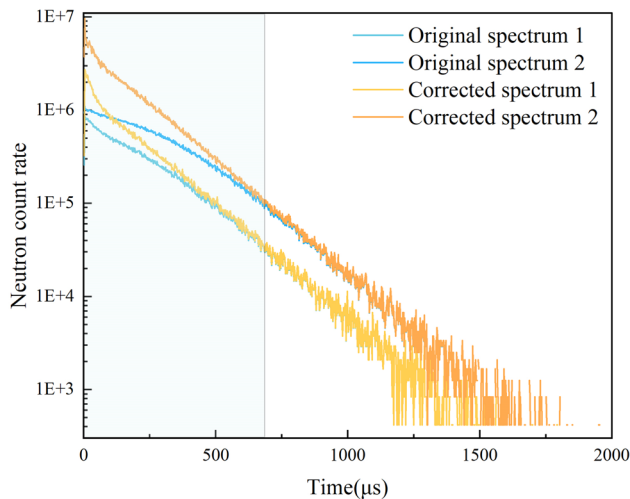


Fig. 9 (Color online) Experimental time spectrum correction results for PFNUL in model wells

rate. According to Eq. (10), the attenuation coefficient μ^* is fitted to the neutron time spectrum before correction and the neutron time spectrum after correction, and the fitting results are shown in Table 7, which shows that the attenuation coefficients μ^* of the two neutron time spectra have a big difference due to the dead time before correction, and the attenuation coefficients of the two curves are close to the same after correction. According to Eq. (11), the two time spectrum’s μ^* before and after correction were computed and compared. The results indicated a significant reduction in *RD* from 29% to 0.49%, which conforms to the theory of neutron attenuation, and it proves that this correction method has a better effect on the correction of the neutron time spectrum of the PFNUL instrument. It proves that this correction method has a good effect on the neutron time spectrum acquisition correction of the PFNUL instrument, which can greatly improve the quantitative measurement accuracy of the uranium logging site.

5 Conclusion

This study introduces a new method for determining the dead time of a ³He detector system for a PFNUL instrument utilizing a controlled D–T neutron generator to produce

neutron time spectrum information collected at two different neutron fluxes in combination with the neutron decay law. The method employs two windows in the measured spectrum, leveraging the neutron decay law and real and observed counts to derive a dead-time calculation formula. It identifies the suitable range for setting distance and size parameters for the two windows in the calculation:

- (1) The neutron flux ratios f_{d1} and f_{d2} for the two time windows W1 and W2 chosen for the dead-time calculation are at least greater than 2.
- (2) To eliminate the effects of the well holes and the source neutrons the initiation time of the W1 is proposed to be about 400 μ s.
- (3) The spacing t_{wd} between the two windows is greater than 200 μ s.

The determined dead time of the ³He detector system is closely aligning calculated by Hashimoto using the variance-mean method (Feynman- α). With this dead-time result, the neutron time spectrum undergoes correction by counting. The fitted results of the corrected neutron time spectrum decay time constants closely resemble each other. When compared with the MCNP simulated neutron time spectrum decay time constants, the average deviation is less than 5%, verifying the accuracy of the dead-time calculation and the effectiveness of the correction method. Finally, the application was done in PFNUL for uranium quantification, and the expected correction effect was achieved for the neutron time spectrum measured in the uranium model wells, and the attenuation coefficients of the corrected two neutron time spectra tended to be consistent, which was in line with the theoretical requirements, and improved the measurement accuracy of the PFNUL instrument for uranium quantification in the field.

Author contributions All authors contributed to the study conception and design. Material preparation, data collection, and analysis were performed by Yan Zhang, Chi Liu, Ren-Bo Wang, Shi-Liang Liu, Hao-Ran Zhang, Hai-Tao Wang, Jin-Hui Qu, Wen-Xing Hu, Ren-Bo Wang, and Bin Tang. Yan Zhang and Chi Liu wrote the first draft of the manuscript, all authors commented on the previous versions of the manuscript. All authors read and approved the final manuscript.

Data availability The data that support the findings of this study are openly available in Science Data Bank at <https://cstr.cn/31253.11.sciencedb.16178> and <https://doi.org/10.57760/sciencedb.16178>.

Declarations

Conflict of interest The authors declare that they have no conflict of interest.

References

1. R.L. Caldwell, Nuclear logging methods. *Radioisotopes* **17**(4), 171–185 (1968). https://doi.org/10.3769/radioisotopes.17.4_171
2. J. Qiu, Y. Zhang, C.Q. Fu et al., Study on photofluorescent uranium ore sorting based on deep learning. *Miner. Eng.* **206**, 108523 (2024). <https://doi.org/10.1016/j.mineng.2023.108523>
3. Y. Jin, F.L. Chen, X.Y. Chai et al., Development and application of nuclear logging technique. *At. Energy Sci. Technol.* **38**, 201–201 (2004). <https://doi.org/10.7538/yzk.2004.38.S1.0201>. (in Chinese)
4. F. Zhang, L.L. Tian, Research development and tendency of controllable neutron and X-ray source well logging technology. *J. Isot.* **32**(3), 133–150 (2019). <https://doi.org/10.7538/tws.2019.32.03.0133>. (in Chinese)
5. Z.G. Yuan, Comparative analysis of nuclear magnetic resonance well logging and nuclear magnetic resonance mud logging. *At. Energy Sci. Technol.* **42**(7), 581–585 (2008). <https://doi.org/10.7538/yzk.2008.42.07.0581>. (in Chinese)
6. H.W. Yu, Y.X. Zhang, X.H. Chen et al., Numerical simulation and method study of X-ray litho-density logging. *Nucl. Sci. Technol.* **31**, 124 (2020). <https://doi.org/10.1007/s41365-020-00826-2>
7. W.M. Yin, H.Z. Liu, B. Tang et al., Determination of uranium-radium equilibrium coefficient of uranium ore sample using characteristic peaks in γ -ray spectrum. *At. Energy Sci. Technol.* **44**(7), 769–772 (2010). <https://doi.org/10.7538/yzk.2010.44.07.0769>. (in Chinese)
8. Z.K. Li, R. Yang, B.S. Hu et al., Reserve prediction method of sandstone uranium reservoir based on data of natural gamma logging while drilling. *At. Energy Sci. Technol.* **55**, 373–379 (2021). <https://doi.org/10.7538/yzk.2021.zhukan.0194>. (in Chinese)
9. Z.F. Liu, C.L. Ding, R.Y. Wang et al., Current status and development trend analysis of neutron logging in uranium mines in China. *J. Phys. Conf. Ser.* **1865**, 022006 (2021). <https://doi.org/10.1088/1742-6596/1865/2/022006>
10. X.G. Wang, G.B. Wang, G.G. Zhang et al., The Monte Carlo simulation of pulsed neutron-fission neutron uranium logging technique. *J. Isot.* **26**, 48–52 (2013). <https://doi.org/10.7538/tws.2013.26.01.0048>. (in Chinese)
11. G. Tian, X.P. Ouyang, H.G. Qu et al., Digital n/γ discrimination measurement of low intensity pulsed neutron. *Nucl. Tech.* (in Chinese) **38**, 060204 (2015). <https://doi.org/10.11889/j.0253-3219.2015.hjs.38.060204>
12. J.A. Czubek, Pulsed neutron method for uranium well logging. *Geophysics* **37**(1), 160–173 (1972). <https://doi.org/10.1190/1.1440244>
13. H.M. Bivens, G.W. Smith, D.H. Jensen, Pulsed neutron uranium borehole logging with prompt fission neutrons, Sandia Labs., Albuquerque, NM (USA) (1976) (Accessed January 19, 2024). <https://www.osti.gov/biblio/7125703>
14. D.R. Humphreys, R.W. Barnard, H.M. Bivens et al., Uranium logging with prompt fission neutrons. *Int. J. Appl. Radiat. Isot.* **34**(1), 261–268 (1983). [https://doi.org/10.1016/0020-708X\(83\)90129-1](https://doi.org/10.1016/0020-708X(83)90129-1)
15. J.W. Müller, Dead-time problems. *Nucl. Instrum. Methods* **112**(1–2), 47–57 (1973). [https://doi.org/10.1016/0029-554X\(73\)90773-8](https://doi.org/10.1016/0029-554X(73)90773-8)
16. H.L. Wu, J.H. Zhang, C.S. Chu et al., Relationship between γ detection dead-time and count correction factor. *At. Energy Sci. Technol.* **49**(1), 162–165 (2015). <https://doi.org/10.7538/yzk.2015.49.01.0162>. (in Chinese)
17. J.L. Yu, L. Hou, Q. Wang et al., Research on calibration method of relative detection efficiency for large number of ^3He detector. *At. Energy Sci. Technol.* **56**(12), 2594–2600 (2022). <https://doi.org/10.7538/yzk.2022.youxian.0186>. (in Chinese)
18. Q. Zhang, L.L. Lin, A fast forward computational method for nuclear measurement using volumetric detection constraints. *Nucl. Sci. Tech.* **35**, 31 (2024). <https://doi.org/10.1007/s41365-024-01393-6>
19. Z.X. He, L.Y. Xu, L.J. Han et al., Control measurement method of range switch for dual GM counter tubes. *Nucl. Tech.* (in Chinese) **47**, 020402 (2024). <https://doi.org/10.11889/j.02533219.2024.hjs.47.020402>
20. R. He, X.Y. Niu, Y. Wang et al., Advances in nuclear detection and readout techniques. *Nucl. Sci. Tech.* **34**, 205 (2024). <https://doi.org/10.1007/s41365-023-01359-0>
21. B. Almutairi, T. Akyurek, S. Usman, Voltage dependent pulse shape analysis of Geiger-Müller counter. *Nucl. Eng. Technol.* **51**(4), 1081–1090 (2019). <https://doi.org/10.1016/j.net.2019.02.008>
22. H.W. Yu, Q.W. Zhang, Z. Wang et al., Standoff calculation and application of azimuthal density logging based on broad-beam γ -ray attenuation. *Nucl. Tech.* (in Chinese) **46**(11), 110503 (2013). <https://doi.org/10.11889/j.0253-3219.2023.hjs.46.110503>
23. L. Zhang, X. Han, H.W. Yu et al., Lithology affects and correction of neutron porosity logging using D-D source. *Nucl. Tech.* (in Chinese) **45**, 050501 (2022). <https://doi.org/10.11889/j.0253-3219.2022.hjs.45.050501>
24. K. Ott, M. Helmecke, M. Luszik-Bhadra et al., Dead-time effects of neutron detectors due to pulsed radiation. *Radiat. Prot. Dosimetry.* **155**(2), 125–140 (2013). <https://doi.org/10.1093/rpd/ncs326>
25. W. Feller, On probability problems in the theory of counters, in *Selected Papers I*, ed. by R.L. Schilling, Z. Vondraček, W.A. Woyczyński (Springer, Cham, 2015), pp.751–759. https://doi.org/10.1007/978-3-319-16859-3_39
26. S.E. Binney, Multiple-decaying-source method for the determination of the dead time of a delayed-neutron counting system. *Nucl. Instrum. Methods Phys. Res. Sect. A* **292**(3), 643–647 (1990). [https://doi.org/10.1016/0168-9002\(90\)90182-6](https://doi.org/10.1016/0168-9002(90)90182-6)
27. A.T. Simone, S. Croft, A. Favalli et al., A comparison of approaches to determine dead time parameters using a Boron-Coated-Straw high-level neutron coincidence counter. *ESARDA Bull. Int. J. Nuclear Safeguards Non-proliferation* **54**, 6–13 (2017). <https://doi.org/10.3011/ESARDA.IJNSNP.2017.2>
28. D.J. Loaiza, High-efficiency ^3He proportional counter for the detection of delayed neutrons. *Nucl. Instrum. Methods Phys. Res. Sect. A* **422**(1), 43–46 (1999). [https://doi.org/10.1016/S0168-9002\(98\)01059-6](https://doi.org/10.1016/S0168-9002(98)01059-6)
29. F. Zhang, Y. Sun, Application of Monte Carlo method in the pulsed neutron logging. *J. Isot.* **18**(Z1), 21 (2005). <https://doi.org/10.7538/tws.2005.18.Z1.0021>. (in Chinese)
30. T. Akyurek, L.P. Tucker, X. Liu et al., Portable spectroscopic fast neutron probe and ^3He detector dead-time measurements. *Prog. Nucl. Energy* **92**, 15–21 (2016). <https://doi.org/10.1016/j.pnucene.2016.06.007>
31. T. Akyurek, A new dead-time determination method for gamma-ray detectors using attenuation law. *Nucl. Eng. Technol.* **53**, 4093–4097 (2021). <https://doi.org/10.1016/j.net.2021.06.038>
32. S.C. Xiang, Y.C. Wang, J.Q. Yuan et al., Deadtime measurement for gamma spectrometer system with Ge detector. *Nucl. Tech.* (in Chinese) **14**(6), 355–358 (1991)
33. K. Hashimoto, K. Ohya, Y. Yamane, Experimental investigations of dead-time effect on Feynman- α method. *Ann. Nucl. Energy.* **23**(14), 1099–1104 (1996). [https://doi.org/10.1016/0306-4549\(95\)00121-2](https://doi.org/10.1016/0306-4549(95)00121-2)
34. Y. Zhang, H.R. Zhang, R.B. Wang et al., Research on passive neutron multiplicity device for ^{240}Pu measurement based on FPGA. *Nucl. Sci. Tech.* **35**, 162 (2024). <https://doi.org/10.1007/s41365-024-01514-1>

35. H. Choi, J. Shin, J. Jang, G. Cho, A modified decaying source method for dead time measurement with non-negligible background counts. *Nucl. Instrum. Methods Phys. Res. Sect. A* **1048**, 168026 (2023). <https://doi.org/10.1016/j.nima.2023.168026>
36. C. Zheng, L.L. Song, Z.H. Ai et al., Determination of dead time for counter rate measuring instrument. *At. Energy Sci. Technol.* **45**(11), 1369–1371 (2011). <https://doi.org/10.7538/yzk.2011.45.11.1369>. (in Chinese)
37. G.W. Smith, Status report on the development of a prompt fission neutron uranium borehole logging technique. Sandia National Lab. (SNL-NM), Albuquerque, NM (United States) (1977). <https://doi.org/10.2172/7322627>
38. Y. Zhang, B. Tang, R.B. Wang et al., Chinese patent 202310274795.4, 16 May 2023 (in Chinese)
39. X.G. Wang, G.B. Wang, G.G. Zhang et al., The Monte Carlo simulation of pulsed Neutron-fission neutron uranium logging technique. *J. Isot.* **26**(1), 48–52 (2013). <https://doi.org/10.7538/tws.2013.26.01.0048>. (in Chinese)
40. H.L. Wu, Y.L. Li, Y. Jin et al., A design of source spacing of the X-ray density logging tool based on numerical simulation. *Nucl. Tech.* (in Chinese) **45**, 100402 (2022). <https://doi.org/10.11889/j.0253-3219.2022.hjs.45.100402>
41. D.W. Luo, H.Y. Wu, Z.H. Li et al., Performance of digital data acquisition system in gamma-ray spectroscopy. *Nucl. Sci. Tech.* **32**, 79 (2021). <https://doi.org/10.1007/s41365-021-00917-8>
42. H.Q. Zhang, B. Tang, H.X. Wu, Pulse amplitude extraction in digital nuclear spectrometer system. *Nucl. Tech.* (in Chinese) **36**, 050401 (2013). <https://doi.org/10.11889/j.0253-3219.2013.hjs.36.050401>
43. Y.L. Ge, B.P. Lu, S. Song et al., Pulsed neutron capture logging pulse sequence design. *Well Logging Technol.* **46**, 410–415 (2022). <https://doi.org/10.16489/j.issn.1004-1338.2022.04.006>. (in Chinese)
44. X.F. Meng, G.S. Guo, L. Zhang et al., Neutron shielding property test with combination detection method based on moderation sphere detectors. *Nucl. Tech.* (in Chinese) **39**, 050201 (2016). <https://doi.org/10.11889/j.0253-3219.2016.hjs.39.050201>
45. A.K. Anbalagan, P.-W. Fang, W.-T. Liu et al., Significance of measured negative dead time of a radiation detector using two-source method for educational purpose. *J. Radiat. Res. Appl. Sci.* **14**, 423–428 (2021). <https://doi.org/10.1080/16878507.2021.1987128>
46. S.F. Dai, Y.G. Liu, Y.P. Yin et al., Measurement of prompt neutron decay constant by single pulsed neutron source. *At. Energy Sci. Technol.* **46**(10), 1189–1192 (2012). <https://doi.org/10.7538/yzk.2012.46.10.1189>. (in Chinese)
47. Q. Zhang, G. Zhang, R. Deng et al., Time-spectrum processing technology of neutron lifetime logging based on regularized non-negative least squares method. *J. Pet. Sci. Eng.* **203**, 108604 (2021). <https://doi.org/10.1016/j.petrol.2021.108604>
48. Y. Zhang, B. Tang, W. Jia et al., Application of the Monte Carlo Library least-squares (MCLLS) approach for chromium quantitative analysis in aqueous solution. *Appl. Radiat. Isotopes* **150**, 39–42 (2019). <https://doi.org/10.1016/j.apradiso.2019.02.018>
49. Y. Zhang, W. Jia, R. Gardner et al., Study on the PGNAA measurement of heavy metals in aqueous solution by the Monte Carlo-Library least-squares (MCLLS) approach. *Appl. Radiat. Isotopes* **132**, 13–17 (2018). <https://doi.org/10.1016/j.apradiso.2017.10.037>
50. Y.H. Lai, H.T. Wang, R. Chen, Real-time correction method of uranium mine caliper based on prompt neutron well logging. *Nucl. Tech.* (in Chinese) **44**, 060402 (2021). <https://doi.org/10.11889/j.0253-3219.2021.hjs.44.060402>
51. X.G. Wang, D. Liu, G.B. Wang, Optimization study of epithermal neutron detector in prompt fission neutron uranium logging. *Nucl. Tech.* (in Chinese) **36**, 060401 (2013). <https://doi.org/10.11889/j.0253-3219.2013.hjs.36.060401>
52. H.R. Zhang, Y. Zhang, W.X. Hu et al., Simulation study of uranium content in uranium yellow cake using the active multiplicity method. *Nucl. Tech.* (in Chinese) **47**, 020202 (2024). <https://doi.org/10.11889/j.0253-3219.2024.hjs.47.020202>
53. B. Tang, R.B. Wang, S.M. Zhou et al., Chinese patent 201310408465.6, 13 Sep 2013 (in Chinese)
54. B. Tang, R.B. Wang, S.M. Zhou et al., Chinese patent 201320592725.5, 2 Apr 2014 (in Chinese)
55. B. Tang, H.T. Wang, R. Cheng et al., Chinese patent 201810076976.5, 6 Aug 2018 (in Chinese)
56. B. Tang, R.B. Wang, S.M. Zhou et al., Chinese patent 201310440359.6. 2013 (in Chinese)

Springer Nature or its licensor (e.g. a society or other partner) holds exclusive rights to this article under a publishing agreement with the author(s) or other rightsholder(s); author self-archiving of the accepted manuscript version of this article is solely governed by the terms of such publishing agreement and applicable law.

Authors and Affiliations

Yan Zhang^{1,2}  · Chi Liu¹  · Shi-Liang Liu¹ · Hao-Ran Zhang¹ · Hai-Tao Wang¹  · Jin-Hui Qu¹ · Wen-Xing Hu¹  · Ren-Bo Wang¹ · Bin Tang¹

✉ Yan Zhang
yanzhang@ecut.edu.cn

✉ Bin Tang
tangbin@ecut.edu.cn

² Fundamental Science on Radioactive Geology and Exploration Technology Laboratory, East China University of Technology, Nanchang 330013, China

¹ National Key Laboratory of Uranium Resources Exploration-Mining and Nuclear Remote Sensing, East China University of Technology, Nanchang 330013, China